Comparison of Bidirectional Transmittance Distribution Function (BTDF) Measurements on Fused Silica and Sintered Polytetrafluoroethylene Diffusers

James J. Butler
NASA Goddard Space Flight Center
Greenbelt, MD 20771

Georgi T. Georgiev
NASA Goddard Space Flight Center
Greenbelt, MD 20771

Catherine C. Cooksey
National Institute of Standards and Technology
Gaithersburg, MD 20899

Abstract:

Accurate determination of the bidirectional transmittance distribution function (BTDF) of transmissive diffusers is critical for the on-orbit spectral radiance calibration of several satellite-based, Earth remote sensing instruments. This study presents the results of the comparison of BTDF measurements by NASA Goddard Space Flight Center's Diffuser Calibration Laboratory and the National Institute of Standards and Technology's Spectral Tri-function Automated Reference Reflectometer facility on two transmissive diffusers: HOD-500, a synthetic fused silica sample manufactured by Hereaus Quarzglas and Spectralon-250, a sintered polytetrafluoroethylene sample manufactured by Labsphere, Incorporated.* BTDF measurements were acquired at seven wavelengths from 290 nm to 740 nm, at incident elevation angles of 0° and 30°, and at scatter elevation angles from 1° to 15°. Comparison of the measurements made by the two facilities revealed excellent agreement within their combined standard uncertainties. NASA chose the parameters for the BTDF measurements to be identical to those NASA used when measuring the BTDF of the flight diffusers to be flown onboard the Tropospheric Monitoring of Pollution (TEMPO) and the Geostationary Environment Monitoring Spectrometer (GEMS) satellite instruments. Successful agreement between NASA and NIST of BTDF results, therefore, effectively validates the BTDF measurements NASA made for these satellite flight programs.

Introduction:

The angular dependence of the optical scatter properties of a material is fully described by its bidirectional scatter distribution function (BSDF). Specialized cases of BSDF include a material's bidirectional reflectance distribution function (BRDF) and bidirectional transmittance distribution function (BTDF). Specifically, the BTDF is a measure of the transmitted optical scatter of a material as a function of wavelength and direction. The directional dependence of BTDF is a function of the incident and scatter elevation and azimuthal illumination angles measured relative to the sample normal. BTDF includes light scattered at the material's two surfaces and by the bulk material itself. As depicted in Figure 1, surface scatter arises from the presence of micro-roughness, scratches, and deviations from a

perfect plane, while bulk scatter arises from the presence of internal striations, bubbles, inclusions, and granularity.

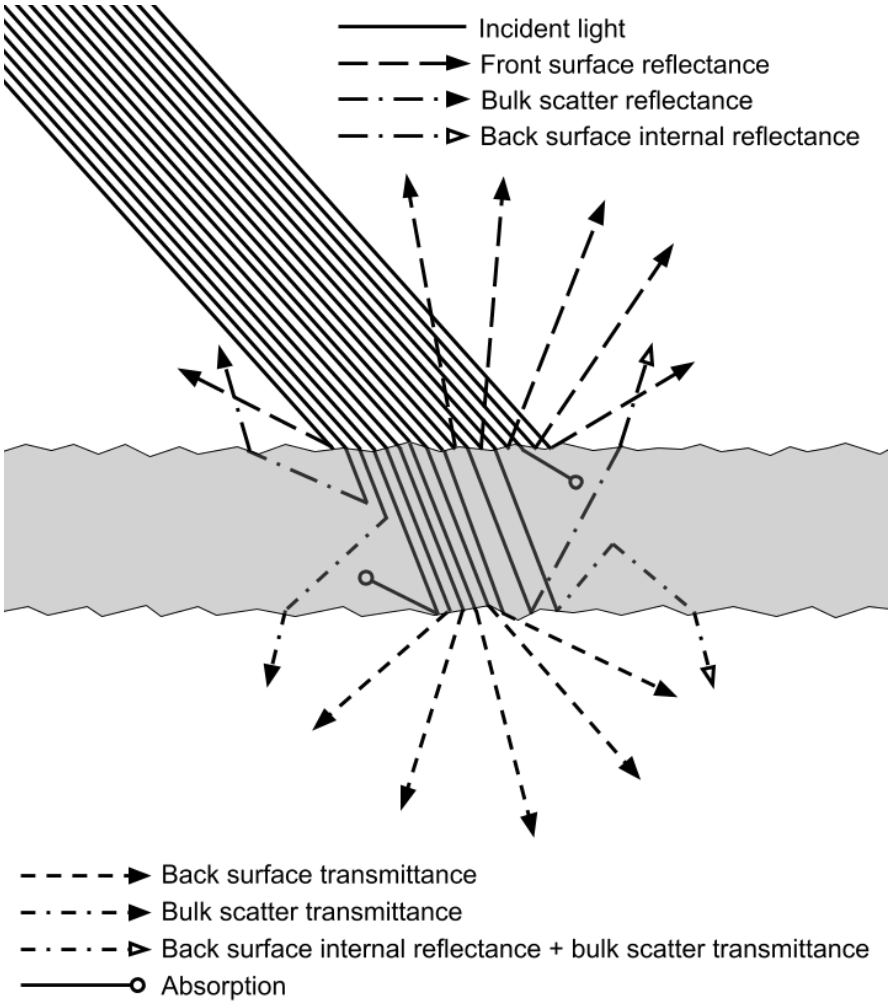

Figure 1. Transmissive diffuser optical scattering. This figure schematically shows the first order interaction of incident light onto a transmissive diffuser including front and back surface scatter. Single bulk scattering and simple absorption processes are also depicted. Second and higher order reflections, transmissions, absorptions, and bulk scattering present in the diffuser are not shown to maintain figure clarity.

The basic concept, methodology, and procedure for the measurement of BTDF was first defined in a paper by Bartell, et al. [1] as a logical extension of the pioneering, reflectance-based work of Nicodemus et al. [2]. Since BTDF provides a quantitative description of the transmitted appearance of materials, there are numerous applications for its measurement including, but not limited to, the fields of architecture and interior design [3-5], computer graphics and rendering [6,7], biomedicine [8-13],

fashion [14], the automotive industry [15], the solar cell industry [16, 17], plant physiology [18-22], and laboratory safety [23].

A number of satellite-based, Earth remote sensing instruments have incorporated transmissive diffusers for the purpose of on-orbit spectral radiance calibration. For example, the Shuttle Solar Backscatter Ultraviolet (SSBUV) instrument, a payload instrument flown on eight space shuttle missions between October 1988 and January 1996, deployed a transmissive solar diffuser comprised of two, 1 mm thick, ground, synthetic crystalline quartz plates in its measurements of spectral solar irradiance [24]. The Ozone Monitoring Instrument (OMI) currently flying on NASA's Earth Observing System (EOS) Aura satellite views a tungsten lamp through a quartz transmissive diffuser for on-orbit flat fielding of the instrument CCD detector, monitoring of instrument throughput, and as an additional optical path for instrument pre-launch characterization [25]. The Ozone Mapping and Profiling Suite (OMPS) limb instrument on the Suomi National Polar-orbiting Partnership (S-NPP) spacecraft employs two transmissive solar diffusers comprised of two roughened diffuse surfaces on fused silica and a microlens assembly to determine on-orbit detector pixel gain [26]. The Orbiting Carbon Observatory-2 satellite instrument uses a transmissive diffuser comprised of a pair of randomly perforated plates facing the sun and instrument telescope with the interior surfaces of the plates textured and gold covered [27]. Lastly, the Tropospheric Monitoring of Pollution (TEMPO) and the Geostationary Environment Monitoring Spectrometer (GEMS) instruments will employ multi-paned quartz transmissive diffusers for on-orbit calibration of their ultraviolet, visible, and near infrared channels.

The application of transmissive diffusers in the calibration of Earth-observing satellite instruments ideally requires diffusers made of a material whose transmittance is uniform, Lambertian, and spectrally flat; stable over all on-orbit operating temperatures; contaminant free; resistant to transmittance degradation; and fluorescence-free under on-orbit solar illumination. Two materials often considered as candidates for on-orbit satellite instrument calibration are roughened natural fused quartz and synthetic fused silica. An excellent description of the composition and metrology of these basic materials is provided in Nurnberg, et al. [28]. Changes in the optical absorption of natural fused quartz following gamma irradiation and heat treatment is presented in Nunes, et al. [29]. Comparison of the directional hemispherical and bidirectional reflectance of both natural fused quartz and synthetic fused silica is provided in Heath and Georgiev [30].

The application of synthetic fused silica transmissive diffusers in remote sensing instrument calibration has driven industry to improve the Lambertian scattering qualities of this material. Examples of these improved synthetic fused silica diffusers include OM and HOD manufactured by Hereaus Quarzglass, Diffusil manufactured by Opsira GmbH, and Primusil OQ manufactured by SGIL Silicaglas GmbH. OM is a high purity quartz glass with evenly distributed micron size pores which invoke diffuse optical scatter when illuminated. HOD, Diffusil, and Primusil are also high-purity fused synthetic quartz glasses, but they are embedded uniformly with microbubbles instead of pores.

Although primarily used as a diffuse reflector, polytetrafluoroethylene (PTFE) is also considered a candidate material for a transmissive diffuser due to its volume scattering properties. Examples of this

material which have been used as transmissive diffusers include Spectralon manufactured by Labsphere, Inc. and Fluorilon-99W manufactured by Avian Technologies.

An important requirement for the use of diffusers in on-orbit satellite instrument calibration, whether in reflective or transmissive mode, is knowledge of the BSDF of the diffusers with a combined standard uncertainty of 1 % or better over typical on-orbit mission lifetimes. Most satellite instruments employ diffusers illuminated by the Sun in reflectance mode. For that reason, the knowledge base for the reflectance of diffusers is much more extensive than that for transmittance. Several publications have addressed the metrology of transmissive scatter through diffusers with specific application to the on-orbit calibration of satellite instruments operating in the ultraviolet through shortwave infrared, including studies of the diffuse transmittance of BTDF OM-100 [30, 31] and HOD-500 and Diffusil-S500 [32].

The most effective method of establishing confidence in the measurement of BTDF (or BRDF) is through measurement comparisons between laboratories using a set of common samples. To identify a set of transmissive diffusers for such a measurement comparison, NASA's Goddard Space Flight Center (GSFC) and the National Institute of Standards and Technology (NIST) reported preliminary results of the directional-hemispherical transmittance and BTDF measurements on several transmissive quartz and Spectralon diffusers as a function of sample thickness and surface treatment [32]. The results of that study led to the selection of HOD-500 and Spectralon-250 as candidate diffusers for this measurement comparison [33].

This paper presents the results for the BTDF comparison by NASA and NIST using the HOD-500 and Spectralon-250 samples. It is believed that this study is the first published inter-laboratory comparison of the measurement of absolute BTDF. The wavelengths and incident and scatter angles chosen for these BTDF measurements are identical to those used by NASA to measure the BTDF of flight diffusers for TEMPO and GEMS satellite instruments in the 2015-2016 timeframe. Successful agreement of the BTDF results by NASA and NIST, therefore, effectively validates the BTDF measurements NASA made for those satellite flight programs.

Method:

The BTDF is defined as the ratio of the transmitted radiance scattered by a sample, $L_{\tau s}$, in a specific direction to the incident irradiance on that sample, E_i [34].

$$BTDF = \frac{L_{\tau s}\,(\theta_i, \emptyset_i, \theta_s, \emptyset_s, \lambda\,)}{E_i(\theta_i, \emptyset_i, \lambda\,)} \qquad (1)$$

In this equation, θ_i is the elevation angle of the incident light measured relative to the top sample normal, +z; ϕ_i is the azimuthal incident angle measured from the sample x axis; θ_s is the elevation angle of the transmitted, scattered light measured from the bottom sample normal, -z; ϕ_s is the azimuthal

angle of the transmitted light measured relative to the sample x axis; and λ is the wavelength of the incident light. Figure 2 illustrates the geometry for the measurement of BTDF of a transmissive sample.

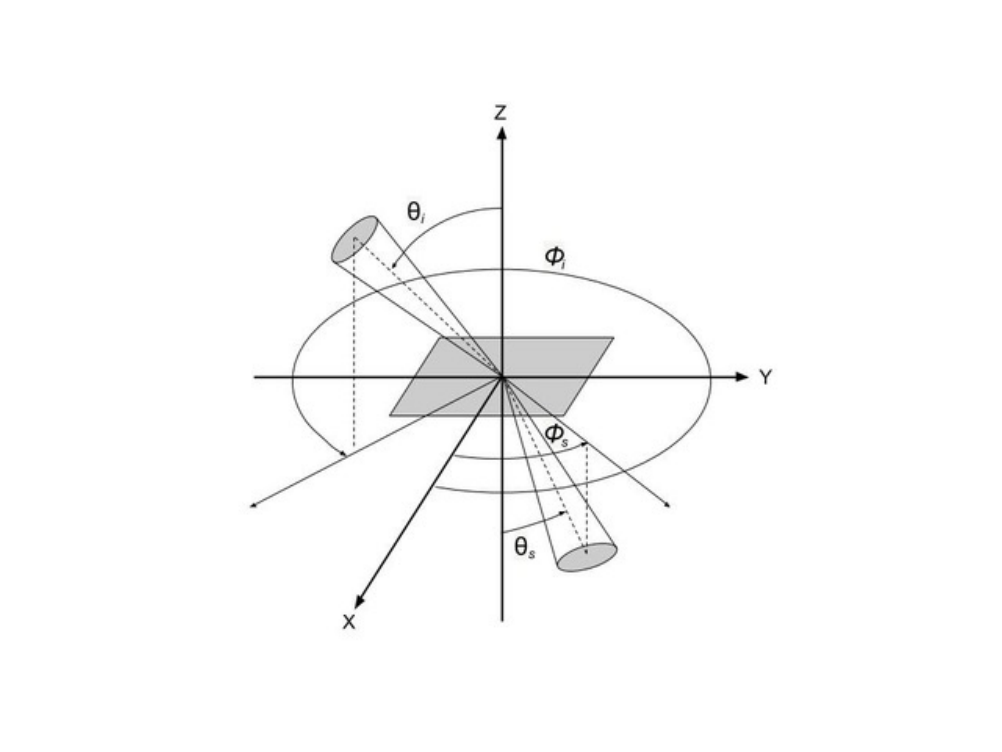

Figure 2. BTDF measurement geometry.

For the case where a relatively small spot on the sample is illuminated and the amount of scattered light is measured into a known solid angle, the BTDF can be defined as the transmitted scattered power per unit solid angle normalized by the product of the incident power and the cosine of the scatter elevation angle [34]. This is illustrated by Equation 2 in which

$$BTDF = \frac{P_s/_{\Omega}}{P_i \cos\theta_s} \qquad (2)$$

P_s is the transmitted scattered power, and P_i is the incident power. Ω is the solid angle determined by the detector aperture area, A, and the distance from the sample to the detector aperture, R, depicted in Equation 3.

$$\Omega = \frac{A}{R^2} \qquad (3)$$

Absolute BTDF measurements were acquired using the scatterometer located in the Diffuser Calibration Laboratory at NASA GSFC and the Spectral Tri-function Automated Reference Reflectometer (STARR) at NIST [35, 36]. Although the NIST STARR and the NASA instruments were originally designed to perform

BRDF measurements, they can be easily programmed to perform BTDF measurements. For this study, the measurement methodology is the same for both instruments. The illumination systems consisted of a lamp coupled to a monochromator to provide wavelength resolution. The detector systems consisted of a precision aperture, field lens, field stop, and a broadband detector. The systems were telecentric and polarization insensitive. Both instruments illuminated and viewed samples under test such that their detector fields-of-view were underfilled. The specific parameters and other details for each instrument can be found in Table 1. Schematics of each instrument are provided in Figures 3 and 4.

For both the NASA and NIST measurements, the samples were aligned such that the incident light and the detector rotated around a common point at the center of each sample's top surface. NASA and NIST absolute BTDF data were acquired and computed around that point for each sample using the following measurement sequence. First, with the sample translated out of the incident beam, the detector was rotated to $\theta_i = 180°$ to measure the incident power, P_i. Then, the sample was returned to the incident position where the source illuminated the center of the top surface of the sample at incident elevation angle, θ_i, defined relative to the sample normal. Variation of θ_i is achieved by rotating the sample about the x axis. Next, the detector was rotated to each scatter elevation angle, θ_s, to measure the transmitted scatter power, P_s.

The measurement parameters for this study are summarized in Table 2. All measurements were in-plane, with incident azimuth, ϕ_i, and scatter azimuth, ϕ_s, angles equal to zero. BTDF measurements for the unpolarized scattering case were obtained by averaging the scatter measurements obtained using using s- and p-polarized incident light.

Table 1. Parameters of each instrument participating in the BTDF comparison

Parameters	NASA GSFC scatterometer	NIST STARR
Measurement Method	Absolute	Absolute
Source	Xenon arc lamp	Xenon arc lamp ($\lambda \leq 400$ nm) QTH lamp ($\lambda > 400$ nm)
Monochromator	0.25 m single grating	0.25 m single grating
Detector	UV-enhanced silicon photodiode	UV-enhanced silicon photodiode
Bandwidth/pass	12 nm	14 nm
Aperture distance	500.0 mm	669.9 mm
Aperture area	160.0 mm^2	796.7 mm^2
Detector solid angle	6.4×10^{-4} sr	1.8×10^{-3} sr
Beam size	13 mm diameter	17 mm diameter

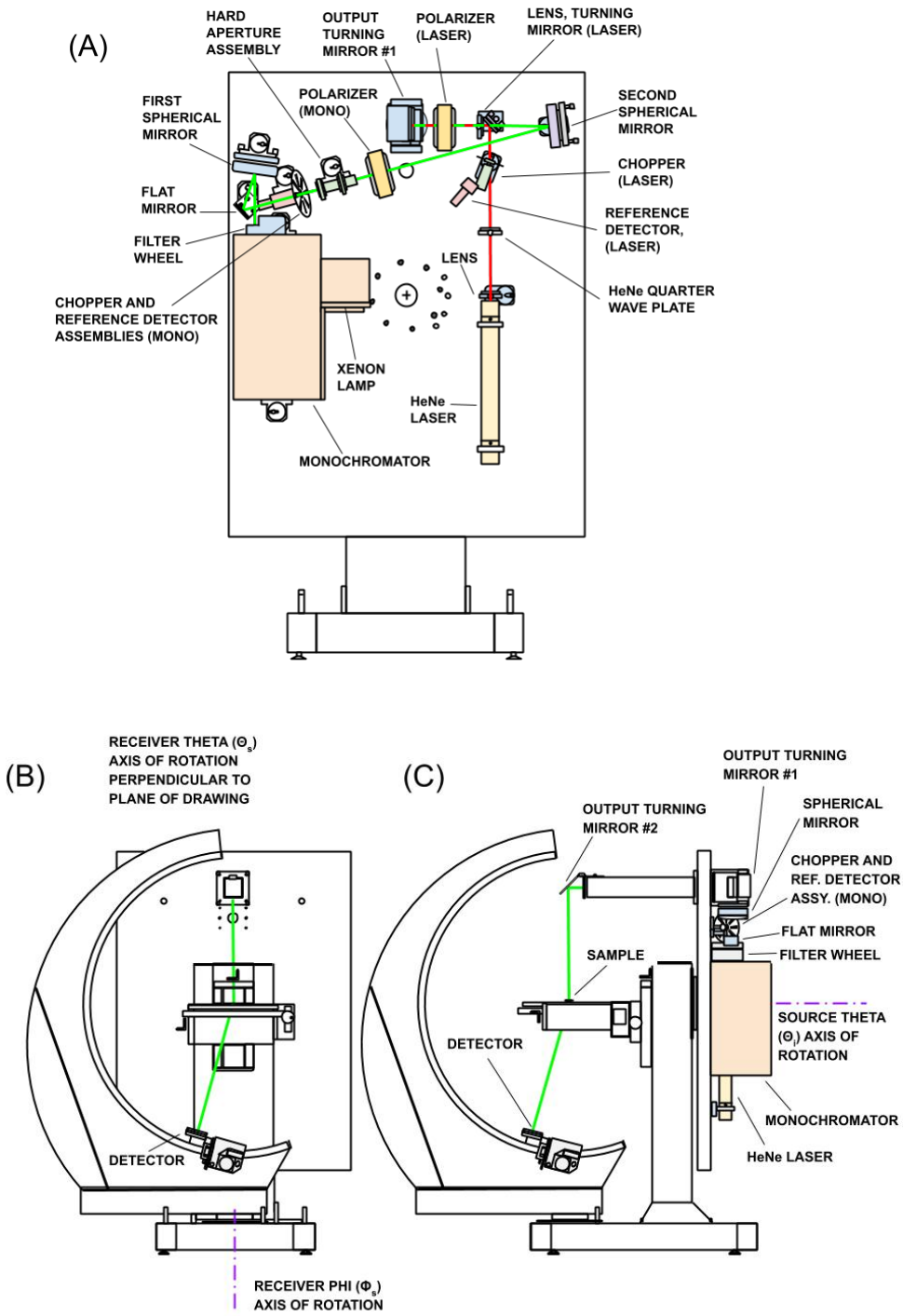

Figure 3. The NASA scatterometer in the BTDF measuring configuration. The light source side of the scatterometer is shown in (A) and the sample side in (B). (C) is a side view showing the sample and light source sides of the instrument with the receiver ϕ stage rotated to a position 90° from that shown in (B). Sample transmitted scatter is measured by the detector looking upward through the sample.

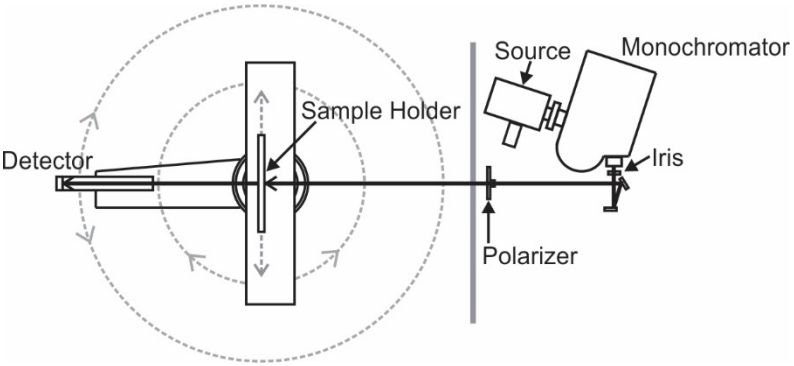

Figure 4. Schematic of NIST STARR's bidirectional measurement system with major components labeled.

Table 2. Measurement parameters for the BTDF measurement comparison

Incident Elevation Angles (θ_i)	Scatter Elevation Angles (θ_s)	Wavelengths	Bandwidths
0° and 30°	1° to 15° in 2° steps	290 nm, 325 nm, 375 nm, 425 nm, 488 nm, 633 nm, 740 nm	NASA: 12 nm NIST: 14 nm

The samples chosen for this BTDF measurement intercomparison were HOD-500 and Spectralon-250. The HOD-500 sample was a monolithic 50.2 mm diameter, 2 mm thick fused silica diffuser manufactured by Heraeus Quarzglas. The sample was fabricated by molding and sintering high purity fused silica powder at high temperature into a solid disk with a uniform internal distribution of microbubbles of less than 25 µm diameter. The use of high purity fused silica powder ensured diffuse performance at ultraviolet wavelengths. The Spectralon-250 sample was a 38.1 mm diameter, 0.25 mm thick sintered PTFE diffuser manufactured by Labsphere, Inc. and mounted between 2 Delrin rings.

BTDF Properties of Samples:

Both NASA and NIST measured the BTDF of HOD-500 and Spectralon-250 samples for the parameters listed in Table 2. Figure 5 displays NASA's measurements of the BTDF of HOD-500 and Spectralon-250 at incident elevation angles of 0° and 30°. The results show that the dependence of BTDF on the scatter elevation angle is small for both samples. Further, the BTDF generally increases as wavelength gets longer.

Figure 6 reveals subtle differences in the Lambertian qualities of the two samples. In this figure, NASA's BTDF measurements of HOD-500 and Spectralon-250 for $\theta_i = 0°$ have been normalized with respect to the BTDF value at $\theta_s = 1°$. The BTDF of Spectralon-250 decreases more rapidly than that of the HOD-500 with increasing scatter elevation angle. This indicates that Spectralon-250 is slightly less Lambertian than HOD-500. A comparison of the plots of Figure 5 also shows that the decrease in BTDF with θ_s is largely independent of wavelength for both samples.

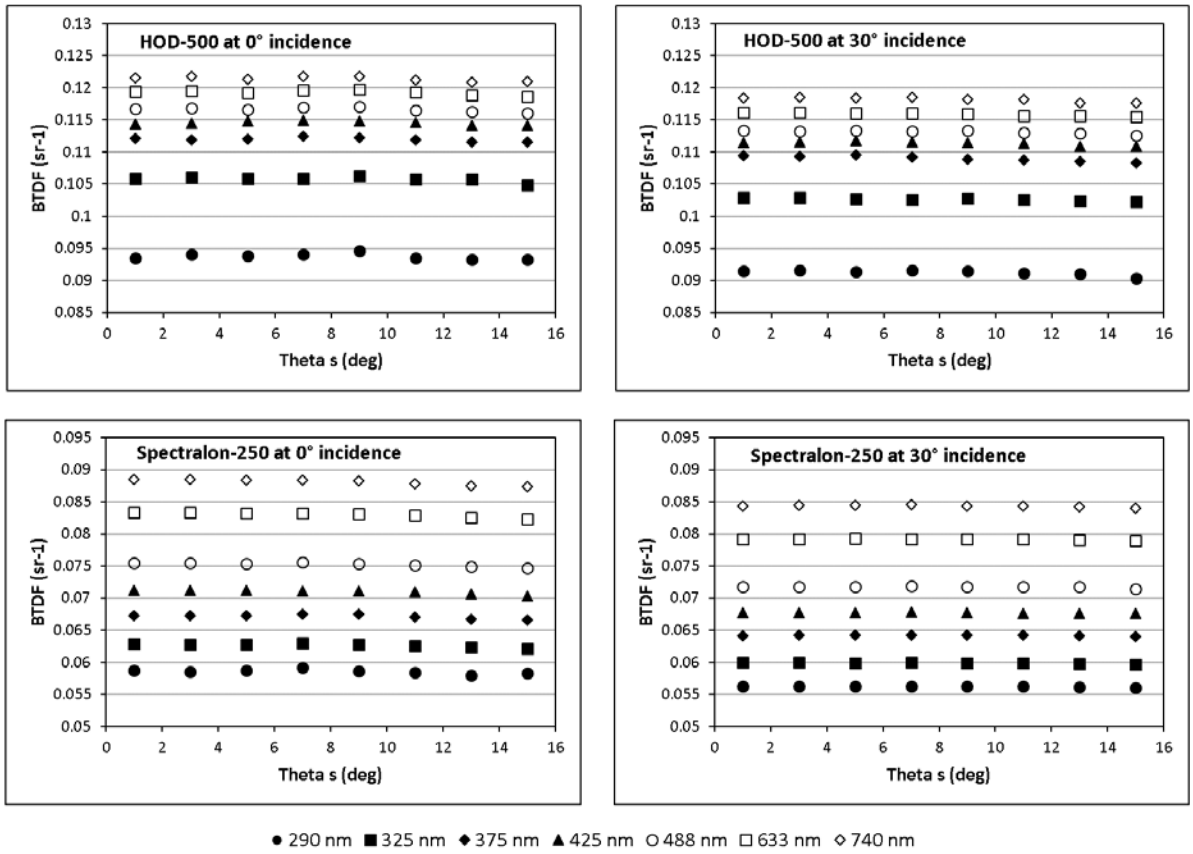

Figure 5. BTDF of HOD-500 and Spectralon-250 measured by NASA at incident elevation angles of 0° and 30°.

Additionally, NASA measured the directional hemispherical transmittance (DHT) of HOD-500 and Spectralon-250 at 0^{o} incidence. These measurements were acquired using a PerkinElmer Lambda1050 spectrophotometer fitted with an integrating sphere accessory. The sphere had a diameter of 150 mm, and an oval entrance port about 15 mm by 25 mm. Each sample was mounted at the entrance port of the integrating sphere, and the size of the illumination spot on the sample was 3 mm by 7 mm. The DHT measurement was acquired for wavelengths from 250 nm to 800 nm with an absolute uncertainty of 0.72 (k=2). The resulting spectra are presented in Figure 7.

The DHT measurements indicate a greater and faster increase in transmittance for HOD-500 compared to Spectralon-250 in the wavelength range from 290 nm to 375 nm. However, for wavelengths longer than 375 nm, the transmittance of HOD-500 increases more slowly than Spectralon-250. Figure 7 also shows scaled BTDF measurements at 0° incidence for both samples. The BTDF values are averaged over all scatter angles from 1° to 15° and multiplied by π. This product of BTDF and π is often referred to as the bidirectional transmittance factor (BTF). In Figure 7, the wavelength dependent behavior of the BTF measurements is qualitatively similar to that observed for the DHT measurements.

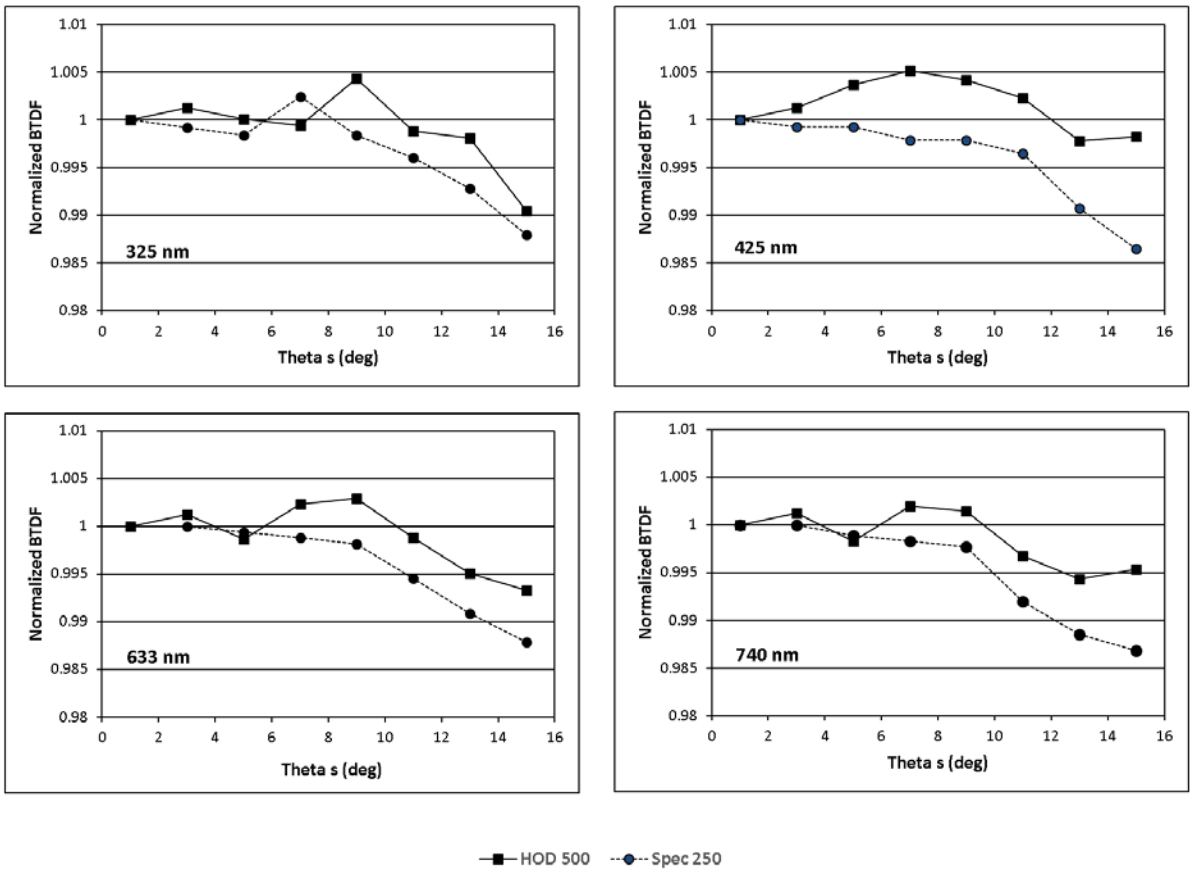

Figure 6. BTDF measured by NASA of the HOD-500 and Spectralon-250 samples as a function of scatter elevation angle θ_s where the BTDF values have been normalized with respect to the value at $\theta_s = 1°$. All values shown here were collected with $\theta_i = 0°$.

NASA-NIST Comparison:

The uncertainty budgets for the NASA and NIST BTDF measurements are presented in Tables 3 and 4, respectively. Both budgets were evaluated in accordance with NIST guidelines and were based on the BTDF measurement equation and instrument variables [35-37]. The sources of uncertainty for the NASA measurements included random effects, detector/electronics nonlinearity, and uncertainties in receiver solid angle, total scatter angle, and wavelength. The uncertainty due to receiver solid angle included uncertainties due to the goniometer arm radius, sample z alignment, and the detector aperture radius. The total scatter angle uncertainty was comprised of uncertainties due to the goniometer scatter angle, sample z alignment, and sample tilt error. The wavelength uncertainty was determined for the shortest wavelength and was applicable to higher wavelengths.

The sources of uncertainty for the NIST measurements were random effects, detector nonlinearity, receiver solid angle, total scatter angle, and wavelength discrimination. The uncertainty component for receiver solid angle included uncertainties due to aperture distance, aperture area, sample location, and approximations made in solid angle calculations. The uncertainty due to approximations in solid angle

calculations account for the finite area of sample illumination and the finite detector collection aperture employed in actual BRDF measurements. Briefly, in this method, an integral for the exact projected solid angle is numerically solved for many combinations of illumination and viewing angles. Those results are compared to the solid angle determined using the simplified method, similar to that used by NASA based on the measured detector to sample distance and aperture area. The average difference in results obtained using the exact and simplified methods is the standard solid angle uncertainty reported by NIST. The total scatter angle uncertainty was comprised of uncertainties due to detector viewing angle and sample location. The uncertainty due to wavelength discrimination was determined for the shortest wavelength and was applicable to higher wavelengths.

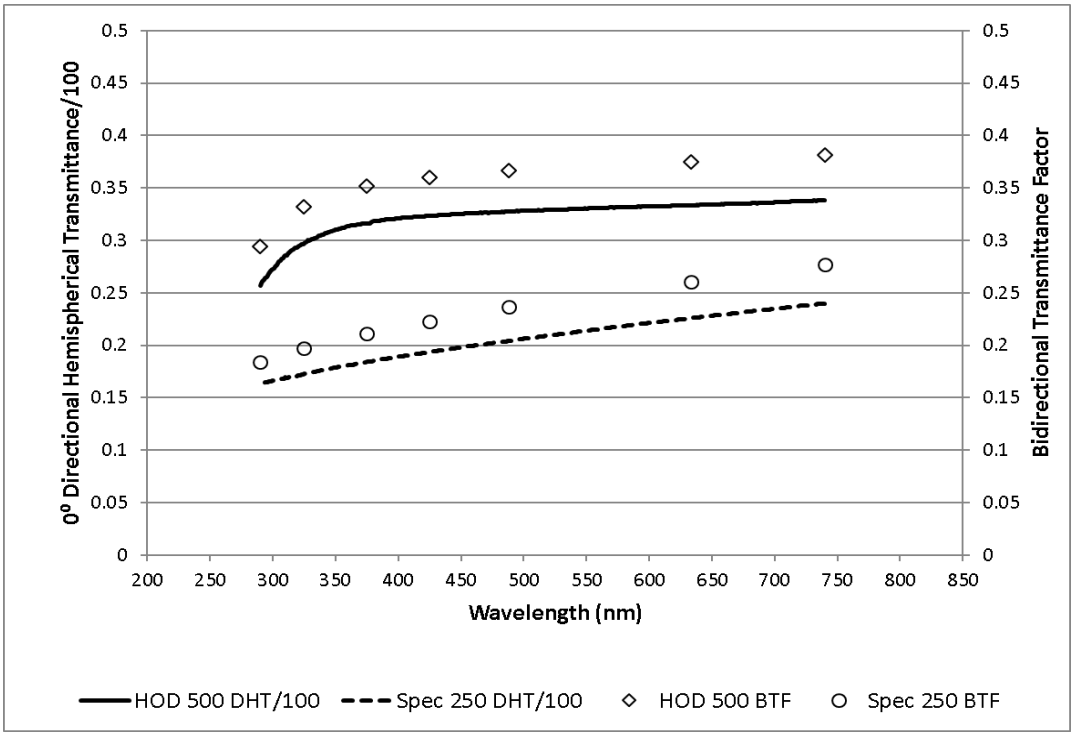

Figure 7. 0^{o} Directional hemispherical transmittance (DHT) of HOD-500 and Spectralon-250. Values for the bidirectional transmittance factor (BTF), which were derived from the 0° incident BTDF data, are provided for qualitative comparison.

Table 3. Relative uncertainty contributions and combined standard uncertainty (k=1) of the BTDF of the HOD-500 and Spectralon-250 samples, as determined by NASA

Source of Uncertainty	Relative Uncertainty Contribution	
	HOD-500	Spectralon-250
Random Effects	0.0010	0.0017
Detector/Electronics Nonlinearity	0.0051	0.0051
Receiver Solid Angle	0.0032	0.0032
Total Scatter Angle	0.0041	0.0041
Wavelength Uncertainty	0.0010	0.0010
	Combined Standard Uncertainty	
	0.0074 or 0.74%	0.0075 or 0.75%

Table 4. Relative uncertainty contributions and combined standard uncertainty (k=1) of the BTDF of the HOD-500 and Spectralon-250 samples, as determined by NIST

Source of Uncertainty	Relative Uncertainty Contribution	
	HOD-500	Spectralon-250
Random Effects	0.0031	0.0017
Detector Nonlinearity	0.0010	0.0010
Receiver Solid Angle	0.0014	0.0015
Total Scatter Angle	0.0004	0.0004
Wavelength Discrimination	0.0052	0.0013
	Combined Standard Uncertainty	
	0.0063 or 0.63%	0.0028 or 0.28%

The NASA and NIST BTDF measurements for each sample and incident elevation angle are presented in Figures 8 through 11. Agreement between NASA and NIST measurements is described quantitatively by calculating the normalized difference between the values of BTDF obtained by each instrument and then comparing the difference to the expanded uncertainty (k = 2) of the two instruments. The normalized differences relative to NIST are calculated according to Equation 4.

$$\Delta_{norm} = \frac{(BTDF_{NASA} - BTDF_{NIST})}{BTDF_{NIST}} \qquad (4)$$

Using Equation 4, the normalized differences in percent of the NASA BTDF data relative to the NIST BTDF data are shown in these figures as the solid circles connected by the dashed lines. The expanded uncertainties, $u(\Delta_{norm})$, are the combined standard uncertainty of the normalized differences multiplied by a coverage factor, k, equal to 2. The $u(\Delta_{norm})$ are calculated according to Equation 5.

$$u(\Delta_{norm}) = \frac{BTDF_{NASA}}{BTDF_{NIST}} \sqrt{(u_{NASA})^2 + (u_{NIST})^2} \times 2 \qquad (5)$$

In equation 5, u_{NASA} and u_{NIST} correspond to the combined standard uncertainties of the NASA and NIST BTDF measurements as presented in Tables 3 and 4. In Figures 8 through 11, the $u(\Delta_{norm})$ are presented in units of sr^{-1} by multiplying the results from Equation 5 by the average of the NASA and NIST BRDF measurements at each scatter angle and plotting the result as error bars centered on that average. Overall, the differences in the NASA and NIST BTDF measurements fall within the expanded uncertainties, indicating excellent agreement between the two instruments. This suggests that each instrument is supported by reasonable uncertainty budgets and substantiates the quality of the BTDF measurements obtained by these instruments.

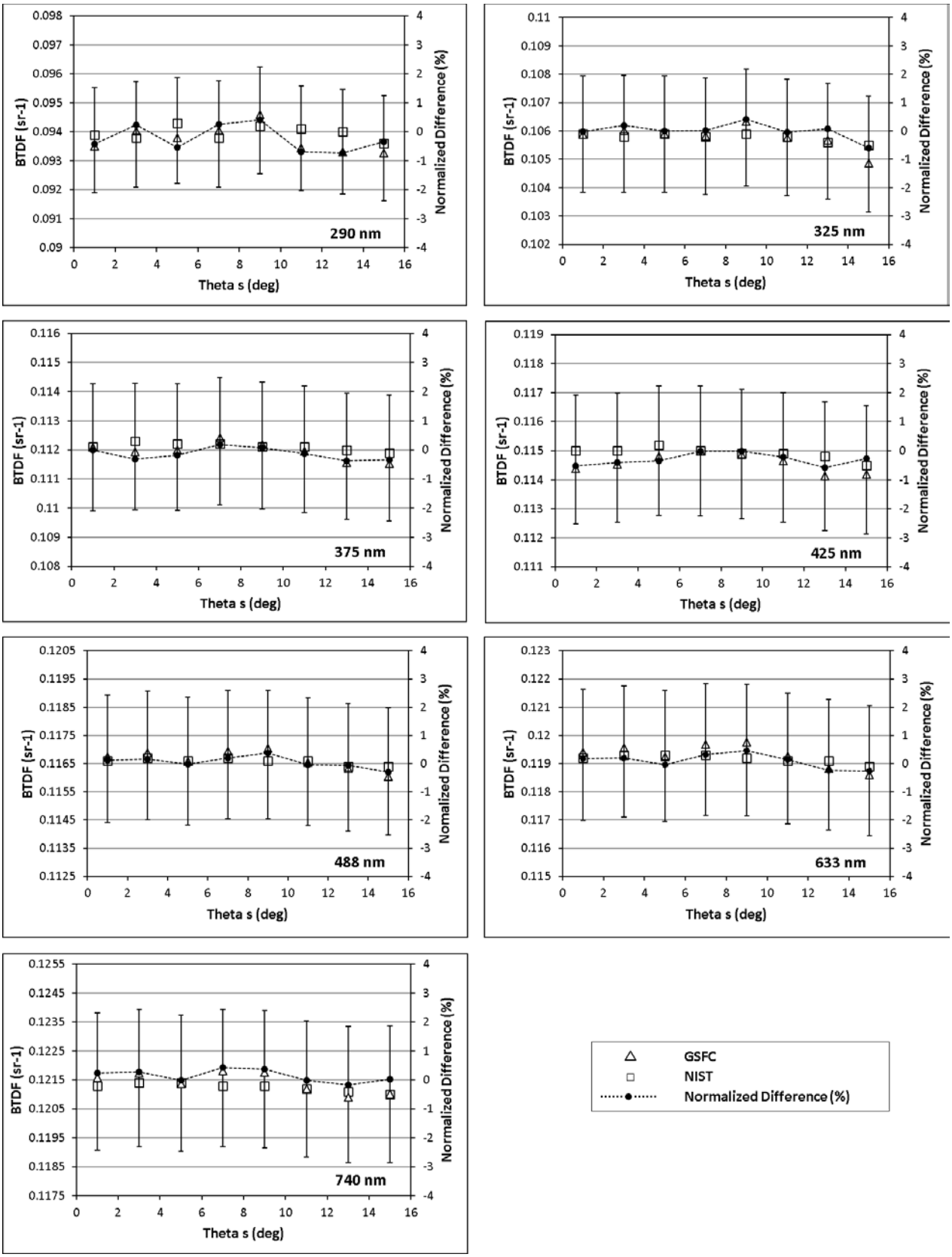

Figure 8. NASA GSFC and NIST BTDF measurements on HOD-500 at θ_i =0° and θ_s=1° to 15°.

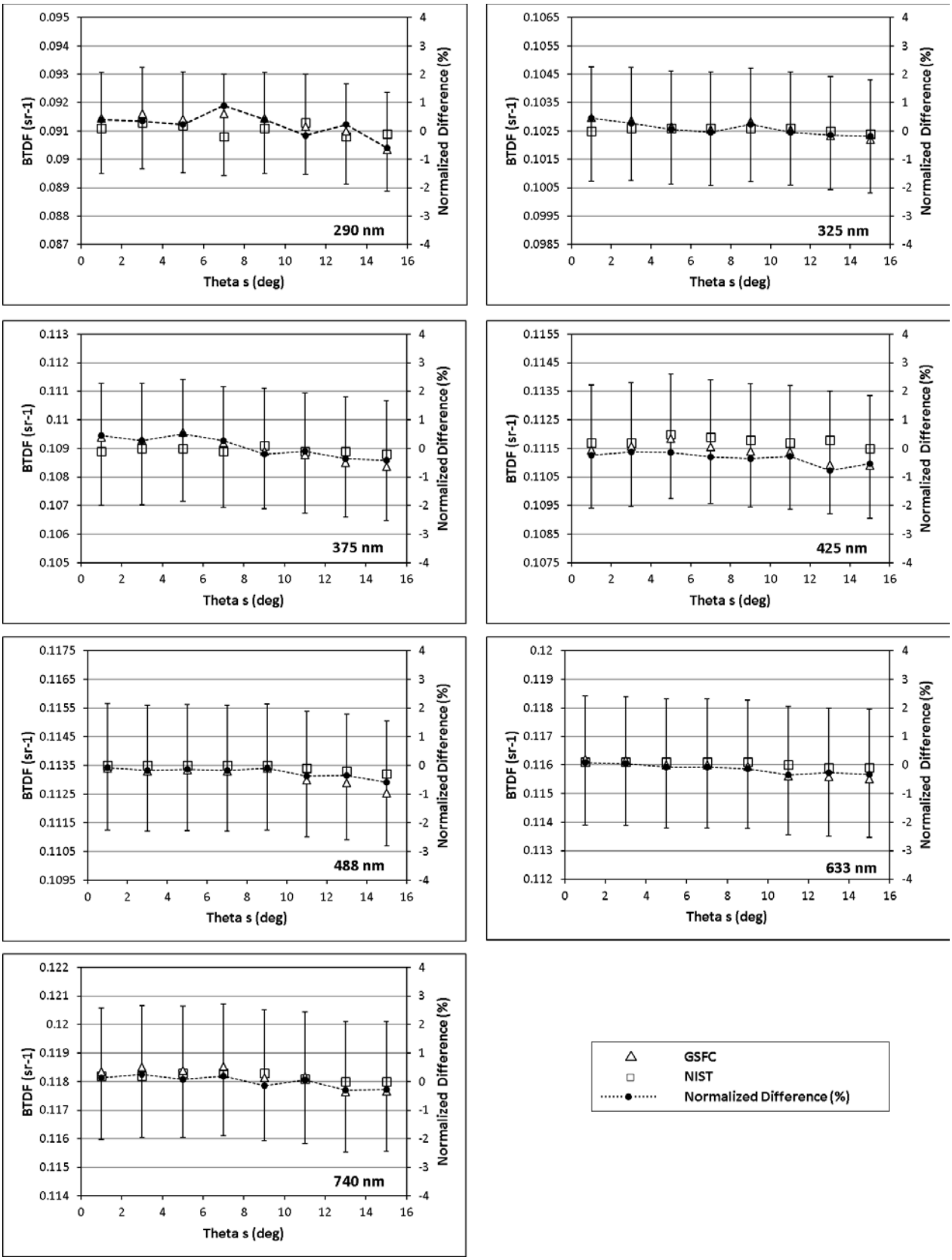

Figure 9. NASA GSFC and NIST BTDF measurements on HOD-500 at θ_i =30° and θ_s=1° to 15°.

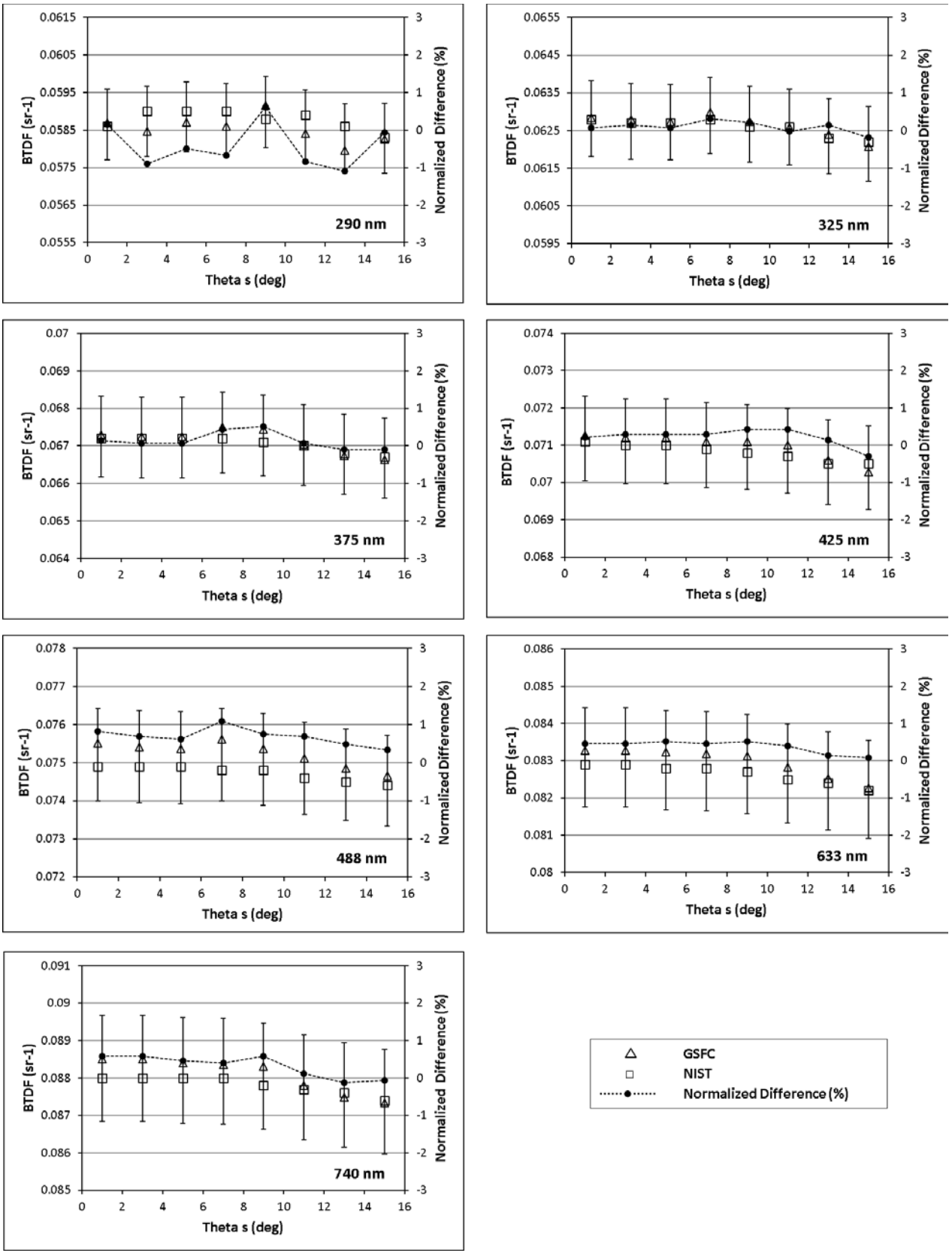

Figure 10. NASA GSFC and NIST BTDF measurements on Spectralon-250 at θ_i =0° and θ_s=1° to 15°.

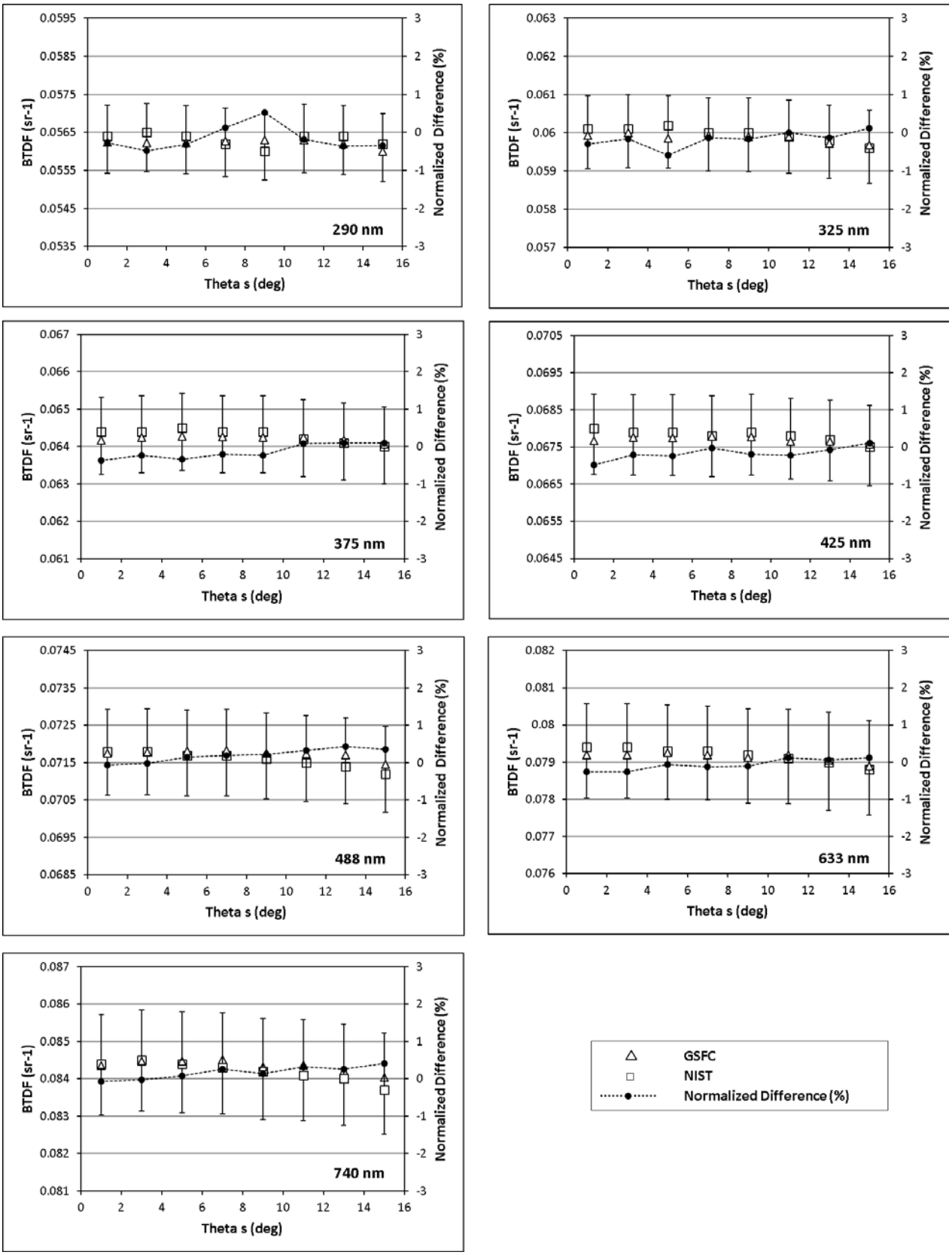

Figure 11. NASA GSFC and NIST BTDF measurements on Spectralon-250 at θ_i =30° and θ_s=1° to 15°.

In accordance with the BRDF comparison study of Early et al. [38], any systematic dependence of NASA's measurements on sample, wavelength, and incident angle was examined by calculating the average normalized difference of the BTDF measurements over all scatter elevation angles at each wavelength. The average normalized differences relative to NIST are shown in Figure 12 as a function of wavelength. The dashed lines represent the expanded uncertainty (k = 2) of the average normalized differences. The resulting average normalized differences for the HOD 500 sample at 0° and 30° incidence and the Spectralon 250 sample at 0° incidence are distributed around 0 %, indicating that any systematic differences between NASA and NIST measurements are small. A small systematic increase with wavelength may be seen in the NASA 0° incident Spectralon 250 data.

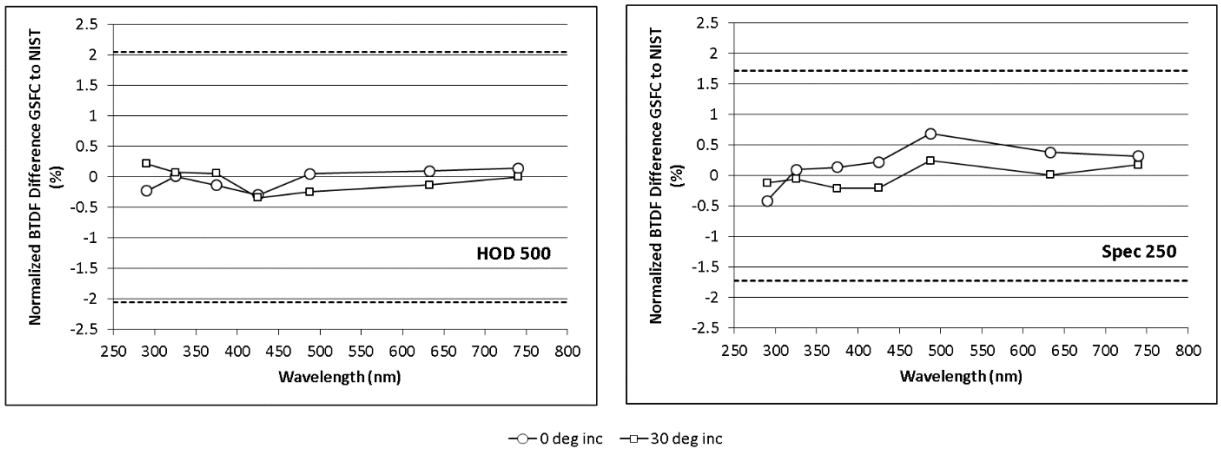

Figure 12. Normalized % difference of BTDF, averaged over all scatter elevation angles, as a function of wavelength measured by NASA relative to NIST. The samples and incident angles are indicated in each panel. The horizontal dashed lines are the expanded uncertainties (k = 2) of the average normalized differences.

Conclusions:

The Diffuser Calibration Laboratory at NASA Goddard Space Flight Center and the Spectral Tri-function Automated Reference Reflectometer facility at NIST measured the BTDF of two transmissive diffusers, HOD-500 and Spectralon-250. The BTDF was measured by each facility at seven wavelengths, namely 290 nm, 325 nm, 375 nm, 425 nm, 488 nm, 633 nm, and 740 nm, at incident elevation angles, θ_i, of 0° and 30° and transmissive scatter angles, θ_s, from 1° to 15° in 2° steps measured from the sample –z axis. The parameters for the BTDF measurements in this comparison were chosen by NASA to be identical to those used by NASA during BTDF measurements of the TEMPO and GEMS flight diffusers in the 2015-2016 timeframe.

Measurements of BTDF, as well as directional hemispherical transmittance, revealed subtle differences in the optical properties of the two samples. BTDF measurements indicate that Spectralon-250 is slightly less Lambertian than HOD-500, and the decrease in BTDF with scatter elevation angle is largely independent of wavelengths for both samples. BTDF, as well as directional hemispherical transmittance,

measurements showed that HOD-500 has higher transmittance values than Spectralon-250 at all measured wavelengths. Additionally, transmittance increases more rapidly with increasing wavelength for HOD-500 than Spectralon-250 in the wavelength range of 290 nm to 375 nm. However, for wavelengths longer than 375 nm, the transmittance for HOD-500 increases more slowly than Spectralon-250.

Comparison of BTDF measurements acquired by NASA and NIST show excellent agreement within the expanded uncertainty. This suggests that each instrument is supported by reasonable uncertainty budgets and substantiates the quality of the BTDF measurements obtained by these instruments. It is believed that this study is also the first published inter-laboratory comparison of the measurement of absolute BTDF.

Because these comparison measurements were acquired with the same parameters used by NASA to measure the BTDF of flight diffusers for TEMPO and GEMS satellite instruments and the BTDF of the HOD-500 sample is similar in magnitude to the BTDF of the flight diffusers, these measurements validate that NASA's uncertainty budget for flight diffusers successfully meets the pre-launch calibration requirement that the BTDF measurements have a combined standard uncertainty of ≤ 1 %.

*Note: Certain commercial equipment, instruments, or materials are identified in this paper in order to specify the experimental procedure adequately. Such identification is not intended to imply recommendation or endorsement by NASA or NIST, nor is it intended to imply the materials or equipment identified are necessarily the best available for the purpose.

References:

1. F.O. Bartell, E.L. Dereniak, and W.L. Wolfe, "The theory and measurement of bidirectional reflectance distribution function (BRDF) and bidirectional transmittance distribution function (BTDF)," Proc. SPIE 257, 154-160 (1981).

2. F.E. Nicodemus. J.C. Richmond, J.J. Hsia, I. N. Ginsberg, and T. Limperis, "Geometrical Considerations and Nomenclature for Reflectance," NBS Monograph 160, October 1977.

3. J.C. Jonsson, M.D. Rubin, A. M. Nilsson, A. Jonsson, and A. Roos, "Optical characterization of fritted glass for architectural applications," Opt. Mat. 31, 949-958 (2009).

4. M. Andersen, M. Rubin, and J-L. Scartezzzini, "Comparison between ray-tracing simulations and bi-directional transmission measurements on prismatic glazing," Solar Energy 74, 157-173 (2003).

5. M. Andersen and J. de Boer, "Goniophotometry and assessment of bidirectional photometric properties of complex fenestration systems," Energy and Buildings, 38, 836-848 (2006).

6. G.V.G. Baranoski and J. G. Rokne, "An algorithmic reflectance and transmittance model for plant tissue," Eurographics '97, 13, 10pp (1997).

7. C. Schlick, “An inexpensive BRDF model for physically-based rendering,” Proc. of the Annual Conference of the European Association for Computer Graphics-Eurographics ’94, 13, 233-246 (1994).

8. A. Krishnaswamy and G.V.G. Baranoski, “A biophysically-based spectral model of light interaction with human skin,” Eurographics 2004, 23, 331-340 (2004).

9. Q. Li, B.J. Lee, Z. M. Zhang, and D.W. Allen, “Light scattering of semitransparent sintered polytetrafluorethylene films,” J. Biomedical Optics, 13, 054064-1-12 (2008).

10. P. Lemaillet, J.P. Bouchard, and D.W. Allen, “Development of traceable measurement of the diffuser optical properties of solid reference standards for biomedical optics at the National Institute of Standards and Technology,” Applied Optics, 54, 6118-6127 (2015).

11. Y. Han, Q. Jia, S. Shen, G. Liu, Y. Guo, X. Zhou, J. Chu, G. Zhao, E. Dong, D.W. Allen, P. Lemaillet, and R. Xu, “Optical characterization of tissue mimicking phantoms by a vertical double integrating sphere system,” Proc. SPIE, 9700, 97000A-1-11 (2016).

12. P. Lemaillet, C. C. Cooksey, Z.H. Levine, A.L. Pintar, J. Hwang, and D.W. Allen, “National Institute of Standards and Technology measurement service of the optical properties of biomedical phantoms: current status,” Proc. SPIE 9700, 97002-1-6 (2016).

13. P. Lemaillet, J.P. Bouchard, J. Hwang, and D.W. Allen,” Double-integrating sphere system at the National Institute of Standards and Technology in support of measurement standards for the determination of optical properties of tissue-mimicking phantoms,” J. Biomedical Optics, 20, 121310-1-8 (2015).

14. T.N. Kocevar and H.G. Tomc, “Modelling and visualization of the optical properties of cloth,” Chapter 3 in Computer Simulation, 45-65 (2017).

15. C. Mockel and J. Scheuchenpflug, “Simulating light in the automobile industry-integrating design and technology,” Photonik International, 88-91 (2008).

16. S. Cainan, S. Neubert, C. Nock, O. Gabriel, M. Rohde, F. Ruske, B. Stannowski, and R. Schlatmann, “Detailed comparison of transparent front contacts for thin film solar cells,” Proc. of the 37th IEEE Photovoltaic Specialists Conference, 579-584 (2011).

17. P. Siffalovic, M. Jergel, M. Benkovicova, A. Vojtko, V. Nadazdy, J. Ivanco, M. Bodik, M. demydenko, and E. Majkova, “Towards new multifunctional coatings for organic photovoltaics,” Solar Energy Materials and Solar Cells, 125, 127-132 (2014).

18. A. Seybold, Planta-Arch. Wissenschaft. Botan., 20, 577 (1933).

19. H.T. Breece III and R.A. Holmes, “Bidirectional Scattering Characteristics of Healthy Green Soybean and Corn Leaves in Vivo,” Applied Optics, 10, 119-127 (1971).

20. L. Grant, “Diffuse and Specular Characteristics of Leaf Reflectance, Rem. Sensing of the Environment, 22, 309-322 (1987).

21. T.C. Vogelmann, “Plant Tissue Optics,” Annual Review of Plant Physiology and Plant Molecular Biology, 44, 231-251 (1993).

22. L. Bousquet, S. Jacquemoud, and I. Moya, “Leaf BRDF and BTDF Measurements and Model,” ISPMSRS 2005 Conference Proceedings, 459-461 (2005).

23. M. Hustedt, C. Hennigs, S. Kalerie, W. Golebiowski, D. Wenzel, and A. Hutter, “Passive and Active Protective Clothing Against Laser Radiation,” Journal of Laser Applications, 25, 042003-1 to 042003-8 (2013).

24. E. Hilsenrath, D. Williams, and J. Frederick, “Calibration of Long Term Data Sets from Operational Satellites Using the Space Shuttle,” Proc. SPIE 924, 215-222 (1988).

25. M.R. Dobber, R.J. Dirksen, P.F. Levelt, G.H.J. ven den Oord, R.M. Voors, Q. Kleipoll, G. Jaross, M. Kowalewski, E. Hilsenrath, G.W. Leppelmeier, J. de Vries, W. Dierssen, and N.C. Roxemeijer, “Ozone Monitoring Instrument Calibration,” IEEE Transactions on Geoscience and Remote Sensing, 44, 1209-1238 (2006).

26. M.G. Dittman, J. Leitch, M. Crisp, J.V. Rodriguez, A. Sparks, B. McComas, N. Zuan, D. Frazer, T. Dixon, R. Philbrick, and D. Wasinger, “Limb Broad-band Imaging Spectrometer for the NPOESS Ozone Mapping and Profiler Suite (OMPS),” Proc. SPIE 4814, 120-130 (2002).

27. D. Crisp, H.R. Pollock, R. Rosenberg, L. Chapsky, R.A.M. Lee, F.A. Oyafuso, C. Frankenberg, C.W. O’Dell, C.J. Bruegge, G.B. Doran, A. Eldering, B.M. Fisher, D. Fu, M.R. Gunson, L. Mandrake, G.B. Osterman, F.M. Schwandner, K. Sun, T.E. Taylor, P. O. Wennberg, and D. Wunch, “The On-orbit Performance of the Orbiting Carbon Observatory-2 (OCO-2) Instrument and its Radiometrically Calibrated Products,” Atmos. Meas. Techniques. 10, 51-81 (2017).

28. F. Nurnberg, B. Kuhn, and K. Rollman, “Metrology of Fused Silica,” Proc. SPIE 10014, 10014F-1 to 10014F-13 (2016).

29. E.H.M. Nunes and F. S. Lameiras, “The Optical Absorption of Gamma Irradiated and Heat-treated Natural Quartz,” Materials Research 8, 305-308 (2005).

30. D.F. Heath and G. Georgiev, “Characteristics of a New Type of Mie Scattering Volume Diffuser and Its Use as a Spectral Albedo Calibration Standard for the Solar Reflective Wavelength Region,” Proc. SPIE, 8153, 81530V-1-81530V-15 (2011).

31. B. Barton, P. Sperfeld, S. Nowy, A. Towara, A. Hope, S. Teichert, G. Hopfenmuller, M. Baer, and T. Kreuzberger, “Characterization of New Optical Diffusers Used in High Irradiance UV Radiometers,” Proceedings of NEWRAD 2011, S. Park and E. Ikonen, eds., 128-129 (2011).

32. P. Lemaillet, H.J. Patrick, T.A, Germer, L. Hanssen, B.C. Johnson, and G.T. Georgiev, “Goniometric and Hemispherical Reflectance and Transmittance Measurements of Fused Silica Diffusers,” Proc. SPIE, 9961, 996109-1-996109-12 (2016).

33. G.T. Georgiev, J.J. Butler, K. Thome, C. Cooksey, and L. Ding, “Preliminary Results of BTDF Calibration of Transmissive Solar Diffusers for Remote Sensing,” Proc. SPIE, 9972, 997205-1-997205-12 (2016).

34. T.A. Germer, J.C. Stover, and S. Schröder, “Angle-Resolved Diffuse Reflectance and Transmittance,” in *Spectrophotometry: Accurate Measurement of Optical Properties of Materials*, T.A. Germer, J.C. Zwinkels, and B.K. Tsai, Eds., Chapter 8 (Elsevier, Amsterdam, 2014).

35. T.F. Schiff, M.W. Knighton, D.J. Wilson, F.M. Cady, J.C. Stover, and J.J. Butler, “A Design Review of a High Accuracy UV to Near Infrared Scatterometer,” Proc. SPIE, 1993, 121-130 (1995).

36. P.Y. Barnes, E.A. Early, and A.C. Parr, “Spectral Reflectance,” NIST Special Publication 250-48, U.S. Department of Commerce, 1998.

37. B.N. Taylor and C.E. Kuyatt, “Guidelines for Evaluating and Expressing the Uncertainty of NIST Measurement Results,” NIST Technical Note 1297, U.S. Department of Commerce, 1997.

38. E.A. Early, P.Y. Barnes, B.C. Johnson, J.J. Butler, C.J. Bruegge, S.F. Biggar, P.R. Spyak, and M.M. Pavlov, “Bidirectional Reflectance Round-robin in Support of the Earth Observing System Program,” J. Atmos. Oceanic Technol., 17, 1077-1091 (2000).